

Conditions for Isoscaling in Nuclear Reactions

M. B. Tsang¹, W.A. Friedman², C.K. Gelbke¹, W.G. Lynch¹, G. Verde¹, H.S. Xu¹

¹ National Superconducting Cyclotron Laboratory and Department of Physics and Astronomy,
Michigan State University, East Lansing, MI 48824

² Department of Physics, University of Wisconsin, Madison, WI 53706

(October 28, 2018)

Abstract

Isoscaling, where ratios of isotopes emitted from two reactions exhibit an exponential dependence on the neutron and proton number of the isotope, has been observed over a variety of reactions including evaporation, strongly damped binary collision, and multifragmentation. The conditions for isoscaling to occur as well as the conditions when isoscaling fails are investigated.

arXiv:nucl-ex/0106009v1 9 Jun 2001

With the availability of rare isotope beams as well as detection systems that can resolve the masses and charges of the detected particles, isotope yields become an important observable for studying nuclear collisions of heavy ions [1,2]. This additional freedom on isospin asymmetry allows one to study the properties of bulk nuclear matter that are affected by the nucleon composition of the nuclei such as the isospin dependence of the liquid gas phase transition of nuclear matter [3,4] and the asymmetry term [5-8] in the nuclear equation of state. To minimize undesirable complications stemming from the sequential decays of primary unstable fragments, it has been proposed that isospin effects can best be studied by comparing the same observables in two similar reactions that differ mainly in isospin asymmetry [4,6,8]. If two reactions, 1 and 2, have the same temperature but different isospin asymmetry, for example, the ratios of a specific isotope yield with neutron and proton number N and Z , obtained from system 2 and system 1 have been observed to exhibit isoscaling i.e. exponential dependence of the form [4,5]:

$$R_{21}(N, Z) = Y_2(N, Z)/Y_1(N, Z) = C \cdot \exp(N \cdot \alpha + Z \cdot \beta) \quad (1)$$

where α and β are the scaling parameters and C is an overall normalization constant. We adopt the convention that the neutron and proton composition of reaction 2 to be more neutron-rich than that of reaction 1.

Figure 1 illustrates the isoscaling property observed with the fragments produced in the central collisions of $^{124}\text{Sn} + ^{124}\text{Sn}$ and $^{112}\text{Sn} + ^{112}\text{Sn}$ reactions [4]. The N and Z dependence of Eq. 1 becomes most apparent if $R_{21}(N, Z)$ is plotted versus N or Z on a semi-log plot as shown in the left panels. Isotopes of the same elements are plotted with the same symbols. Odd- Z nuclei are represented by open symbols while the even- Z nuclei are represented by closed symbols. In the upper left panel, the isotopes for each element Z appear to lie on one line and the resulting slopes would then be α . The dashed (for odd- Z elements) and solid (even- Z elements) lines are best fits to the data points with one common α values for all the elements. In this case, $\alpha = 0.361$. Similarly, plotting $R_{21}(N, Z)$ against Z for all isotones would provide a common slope β for each N . This is demonstrated in the lower

left panel of Figure 1. The best fits (dashed and solid lines) yield a value of $\beta = -0.417$. The positive (negative) slopes of the lines in the top (bottom) panel arise from the fact that more neutron-rich (proton-rich) nuclei are produced in the more neutron-rich (proton-rich) system which represent the values in the numerators (denominators) of the ratios in Eq. 1.

Alternatively, the data in the left panels can be displayed compactly as a function of one variable, either N or Z , by removing the dependence of the other variable using the scaled isotope or isotone functions [6]:

$$S(N) = R_{21}(N, Z) \times \exp(-\beta Z). \quad (2)$$

$$S(Z) = R_{21}(N, Z) \times \exp(-\alpha N). \quad (3)$$

For the best fit value of $\beta (= -0.417)$, $S(N)$ for all elements lies on a single line on a semi-log plot as a function of N as shown in the upper right panel of Figure 1. Alternatively, $S(Z)$ of all isotones lies on a single line on a semi-log plot as a function of Z for the best fit value of $\alpha (= 0.361)$ as shown in the lower right panel. Both solid lines shown in the right panels have the same exponential dependence on N and Z as the corresponding lines in the left panels. The agreement between the data and the lines is excellent, verifying the scaling relation of Eq. 1-3. In general, the fit for $S(N)$ is better than $S(Z)$; this may reflect the influence of Coulomb interaction which may not be well approximated by Eq. 1 [6,8]. On the other hand, $S(N)$ is affected mainly by the differences in neutron chemical potentials or the neutron separation energies. These latter factors may be governed by the differences in the symmetry energies in the two systems [8].

In a recent survey of heavy ion induced reactions, isoscaling appears to be manifested in a variety of nuclear reactions including deeply inelastic collisions, evaporation and multi-fragmentation over a wide range of incident energies [6]. In this article, we will perform a comprehensive exploration of many reactions and examine conditions under which isoscaling is observed and others where it is not. We will also demonstrate how isoscaling can be restored even when two systems have different temperatures.

I. DEEPLY INELASTIC COLLISIONS

In the 1970's, the Deeply Inelastic Collision (DIC) phenomenon was discovered when heavy ions were used to bombard heavy targets in an effort to create superheavy elements [9, 10]. Products from the DIC exhibit characteristics which can partly be attributed to compound nuclei decay and partly to multinucleon transfer reactions depending on the incident energy and detection angles. In ref. [6] the isotope yield ratios of $^{16}\text{O} + ^{232}\text{Th}$ and $^{16}\text{O} + ^{197}\text{Au}$ reactions at incident energy of 137 MeV and $\theta = 40^\circ$ have been found to exhibit isoscaling behavior. From the literature, we have selected four additional systems to illustrate the compliance or noncompliance of the scaling behavior in DIC. Each pair of the chosen reactions use the same projectile at the same incident energy and detect the isotopes at the same laboratory angles. The main differences are the targets. Figure 2 shows the relative isotope ratios, $R_{21}(N, Z)$ for the four systems: a.) $^{16}\text{O} + ^{232}\text{Th}$ [9] and $^{16}\text{O} + ^{197}\text{Pb}$ [10] at incident energy of 137 MeV and $\theta = 40^\circ$ (upper left panel), b.) $^{14}\text{N} + ^{100}\text{Mo}$ and $^{14}\text{N} + ^{92}\text{Mo}$ at 97 MeV and $\theta = 25^\circ$ (upper right panel) [9], c.) $^{22}\text{Ne} + ^{232}\text{Th}$ and $^{22}\text{Ne} + ^{94}\text{Zr}$ at 173 MeV and $\theta = 12^\circ$ [9] (lower left panel), and d.) $^{16}\text{O} + ^{232}\text{Th}$ and $^{16}\text{O} + ^{197}\text{Au}$ at 315 MeV and $\theta = 40^\circ$ (lower right panel) [10]. Isotopes of the same elements are plotted with the same symbols using the same convention as Figure 1, open circles, closed circles, open square, closed squares, and open diamonds for $Z=3, 4, 5, 6,$ and $7,$ respectively. The solid and dotted lines connect isotopes of the same elements (solid lines for even Z element and dashed line for odd Z elements). Scaling similar to Equation 1 is observed for the isotope ratios plotted in the upper panels. When the product nuclei are detected at very forward angles, such as the isotope ratios from the ^{22}Ne induced reactions shown in the lower left panel, scaling is not observed. When the incident energy is raised to 20 MeV per nucleon, target dependence is much weaker than at lower energies [10] and production of isotopes at forward angles is consistent with fragmentation of the projectile and shows no target dependence. In that case, $\alpha = 0, \beta = 0$ and $R_{21}(N, Z) \approx 1$ is observed (lower right panel).

Figure 2 summarizes that isotopic scaling is reasonably well respected at low incident energies ($E/A < 10\text{MeV}$) and at angles backward of the grazing angles but poorly respected

at forward angles. The situation at higher energies is not clear. Isoscaling may have been observed with very small values of α and β . The positive observation of isoscaling can be understood as follows: Backward of the grazing angles, it is often assumed that equilibrium is established between the orbiting projectile and target. In such cases, the isotopic yields follow the "Q_{gg}-systematics" [9,10], in which the primary isotope yield of the projectile-like fragment depends mainly on the Q-value of the mass transfer and can be approximated by

$$Y(N, Z) \propto \exp((M_P + M_T - M'_P - M'_T)/T) \quad (4)$$

where M_P and M_T are the initial projectile and target masses, and M'_P and M'_T are the final masses of the projectile- and target-like fragment. Here, T has a natural interpretation as the temperature, but is not always assumed to be so. Applying charge and mass conservation, and expressing explicitly only the terms that depend on N and Z , one can write $R_{21}(N, Z)$ as

$$R_{21}(N, Z) \propto \exp[(BE(N_2 - N, Z_2 - Z) - BE(N_1 - N, Z_1 - Z))/T], \quad (5)$$

where Z_i and N_i are the total proton and neutron number of reaction i . BE is the binding energy of a nucleus. Expanding the binding energies in Taylor series, one obtains an expression of the form

$$BE(N_2 - N, Z_2 - Z) - BE(N_1 - N, Z_1 - Z) \approx a \cdot Z + b \cdot N + c \cdot Z^2 + d \cdot N^2 + e \cdot ZN, \quad (6)$$

where a, b, c, d , and e are constants from the Taylor expansion. Evaluating Eq. 6 within the context of a liquid drop model, one finds that the second order terms are of the order $(1/A)$, where A is the mass number, relative to the first order terms. The leading order parameters, a and b can be interpreted as the differences of the neutron and proton separation energies for the two compound systems, i.e. $a = -\Delta s_n$ and $b = -\Delta s_p$. Equation 5 can then be approximated as

$$R_{21}(N, Z) \propto \exp[(-\Delta s_n \cdot N - \Delta s_p \cdot Z)/T]. \quad (7)$$

Eq. 7 confirms the earlier studies which showed that the symmetry contribution in Δs_n of the various isotopes associated with the same element, is approximately linear in the number of neutrons transferred. Similarly, Δs_n shows a linear dependence on the charge transferred due to Coulomb-barrier effects [10, 11]. Comparison of Eqs. 1 and 7 reveals that the difference in the average separation energies, $\Delta s_n/T$ and $\Delta s_p/T$, plays a corresponding role to the fitting parameters of α and β . From the binding energy expansion in Eq. 6, one expects that Eq. 7 becomes less accurate and eventually breaks down leading to a failure in isoscaling when the range of fragment masses considered becomes large.

To explore how good is the approximation of using the nucleon separation energies, we calculate R_{21} obtained with Eq. 7 as well as using the exact expression of Eq. 5. We use the two parent systems that describe the $^{16}\text{O} + ^{197}\text{Au}$ and $^{16}\text{O} + ^{232}\text{Th}$ reactions corresponding to $(N_1, Z_1) = (126, 87)$ and $(N_2, Z_2) = (150, 98)$. The deviations, $R_{21}(\text{Eq. 7})/R_{21}(\text{Eq. 5})$ are plotted in Figure 3 for Li, Be, B, C, N and O isotopes as a function of the neutron excess ($N-Z$). Within each element, the deviations assume a parabola shape with the minima located at the neutron rich side of the $N=Z$ line. Over the range of nuclei measured experimentally, $|N - Z| < 3$, the overall deviations are less than $\pm 5\%$. However, this comparison suggests that isoscaling will break down for isotopes with large Z and for nuclei with extreme isospin asymmetry. It appears likely that first order deviations from the scaling behavior can be corrected using functions similar to the parabola shown in Figure 3.

II. COMPOUND NUCLEUS DECAY

The scaling behavior for fragments evaporated from an excited compound nucleus has been discussed in ref. [6]. The measured isotope ratios for $^4\text{He} + ^{116}\text{Sn}$ and $^4\text{He} + ^{124}\text{Sn}$ collisions at $E/A = 50\text{MeV}$ [12] are plotted in Figure 4 using the same convention of Figure 1 and 2. At back angles ($\theta = 160^\circ$, left panel), the isotope ratios of different elements have similar slopes and adjacent elements are separated nearly equi-distance from each other, typical behavior of isoscaling as evidenced by the best fit solid and dashed lines. However, at forward angles ($\theta = 12^\circ$) where contributions from pre-equilibrium processes become significant, isoscaling is not well respected as shown in the right panel. Not only do different

elements have different slopes but also the distances between adjacent isotones vary greatly [12]. In general, there is a tendency for the slope to become steeper as the fragment mass is increased, consistent with the heavier elements emitted at lower temperature. However for the carbon isotope yields, the trend is actually not monotonic with N , indicating a clear failing of isoscaling. More detailed discussions on the forward angle data can be found in Ref. [12] suggesting that the failure of isoscaling may arise from non-equilibrium emission.

The origin of isoscaling for evaporation process follows similar derivations involving the expansion of the binding energies in the Taylor series as described in previous section, resulting in a formula similar to Eq. (7).

$$R_{21}(N, Z) \propto \exp[(-\Delta s_n + \Delta f_n^*) \cdot N - (\Delta s_p + \Delta f_p^* + \Delta\Phi) \cdot Z]/T]. \quad (8)$$

where f_n^* and f_p^* are the neutron and proton excited free energy and Φ is the electrostatic potential at the surface of a nucleus. A full derivation of Eq. (8) can be found in Ref. [6].

III. MULTIFRAGMENTATION PROCESS

The scaling phenomenon was first observed in multifragmentation process in the central $^{124}\text{Sn} + ^{124}\text{Sn}$ and $^{112}\text{Sn} + ^{112}\text{Sn}$ collisions[4] as demonstrated in Figure 1 and discussed in detail in the introduction section. To obtain guidance of how the nuclei yield ratios may be systematized, we examine the dependence of the isotopic yields within the equilibrium limit of the Grand-Canonical Ensemble [13,14]. In this case predictions for the observed isotopic yield are governed by both the neutron and proton chemical potentials, μ_n and μ_p and the temperature T_i , plus the individual binding energies, $BE(N, Z)$, of the various isotopes [11,12].

$$Y_i(N, Z, T_i) = F_i(N, Z, T_i) \cdot \exp(N \cdot \mu_n/T_i + Z \cdot \mu_p/T_i) \cdot \exp(BE(N, Z)/T_i) \quad (9)$$

The factor $F_i(N, Z, T_i)$ includes information about the secondary decay from both particle stable and particle unstable states to the final ground state yields. If the two reactions have the same temperature, ($T_i = T$) the binding energy terms in Eq. (9) cancel out. If one further assumes that the influence of secondary decay on the yield of a specific isotope is

similar for the two reactions, i.e. $F_1(N, Z, T) \approx F_2(N, Z, T)$, then we obtain an equation in the same form as Eq. (1):

$$R_{21}(N, Z) = C \cdot \exp(N \cdot \Delta\mu_n/T + Z \cdot \Delta\mu_p/T) \quad (10)$$

where $\alpha = \Delta\mu_n/T$ and $\beta = \Delta\mu_p/T$ reflect the differences between the neutron and proton chemical potentials for the two reactions and C is an overall normalization constant. $\Delta\mu_n$ and $\Delta\mu_p$ correspond to Δs_n and Δs_p of Eq. 7. Simulations adopting microcanonical and canonical [8] multifragmentation models show that Eq. 10 is respected. Recent SMM model calculations [15] indicate that μ_n and s_n are closely related ($\mu_n \approx -s_n + f_n^*$) for $0 \leq T \leq 3MeV$, where the decay configurations are mainly binary, but the connection between μ_n and s_n becomes increasingly weak as the role of multifragment decay configurations becomes important. These calculations also verify the insensitivities of isoscaling to the effect of sequential decays [8].

IV MIXED SYSTEMS

The isoscaling described by Eq. 1 relies on the emission mechanisms for the fragments in each reaction being described statistically with some common effective temperature and that distortions from secondary decays cancel[4,6,8,16,17]. The exhibition of the systematic trends does not imply that both reacting systems proceed with the same reaction mechanism. This point was demonstrated in Ref. [18] where isotopic yields of fragments produced in central $Au + Au$ multifragmentation process at $E/A = 35MeV$ [19] can be related approximately via isoscaling to those produced in lower multiplicity evaporation process produced in $Xe + Cu$ reactions at $E/A = 30MeV$ [20]. Isoscaling arises because the temperatures for the two reactions are nearly the same i.e. $T_1 \approx T_2$, [21] even though the emission mechanisms in the two reactions differ significantly [19,20].

For reactions which differ mainly in temperatures, isoscaling is also destroyed because the binding energy terms in Eq. 9 do not cancel even if the effect of sequential decays can be neglected.

$$R_{21}(N, Z) = C \cdot \exp(N \cdot \alpha' + Z \cdot \beta') \exp(BE/T_2 - BE/T_1) \quad (11)$$

where $\alpha' = \alpha - k\mu_{n2}$ and $\beta' = \beta - k\mu_{p2}$; $k = 1/T_1 - 1/T_2$. While the new scaling parameters α' and β' are related to α and β , they do not have simple physics interpretations. The left panel of Figure 5 shows the R_{21} ratios extracted from isotope yields of $^{124}\text{Sn} + ^{124}\text{Sn}$ and $^4\text{He} + ^{124}\text{Sn}$. Even though the comparison of the two $\text{Sn} + \text{Sn}$ reactions and the two alpha induced reactions exhibit isoscaling as seen in Figs. 1 and 4, respectively, there is no observable scaling in these systems with different temperatures.

Isoscaling could be restored if $R_{21}(N, Z)$ in Eq. 11 is multiplied by the Boltzmann factor with binding energy and temperatures, $\exp(k * BE(N, Z))$. Previous studies suggest that the temperature of the multifragmentation reaction of $^{124}\text{Sn} + ^{124}\text{Sn}$ collision is about 5 MeV [22] and the temperature of the evaporation reaction of $^4\text{He} + ^{124}\text{Sn}$ is about 3 MeV [12], we obtain $k \approx 0.12$. In Figure 4, $R_{21}(N, Z) \exp(0.12 * BE)$ obtained from the same data plotted in the left panel exhibit very nice systematic behavior shown in the right panel. The restored isoscaling is clearly demonstrated by the dashed and solid lines which are the best fits through the data points with $\alpha' = 0.939$.

Currently, most temperature measurements depend on selected isotope yields e.g. the $T_{iso}(\text{HeLi})$ depends on the yields of $^3,4\text{He}$ and $^6,7\text{Li}$ [2,23,24] and $T_{iso}(\text{CLi})$ relies on the yields of $^{11,12}\text{C}$ and $^6,7\text{Li}$ [23]. Discrepancies in temperature measurements have been observed between $T_{iso}(\text{HeLi})$ and $T_{iso}(\text{CLi})$ [23]. Furthermore, temperatures derived from excited states (T_{ex}) disagree with isotope yield temperatures (T_{iso}) obtained from central collisions at incident energy greater than 35 MeV [23,24]. Such discrepancies could arise if the light charged particles with $Z \leq 2$ are emitted early and/or the emitting sources are not thermalized [20]. With the temperature corrected isoscaling (Eq. 11), the internal consistency of the temperature measurements and the degree of thermalization as a function of incident energy can be investigated further using all the isotopes measured instead of selected isotopes.

In summary, we have surveyed many reactions with different reaction mechanisms. We found that isoscaling occurs if both reactions can be described by statistical reaction mechanisms and that the temperatures of both reactions are nearly the same. However, isoscaling does not yield any information about the reaction mechanisms. In order to draw correct

conclusions from isotopic measurements, it is therefore absolutely essential to obtain additional experimental information that elucidates the underlying reaction mechanism. If the temperatures for both reactions are different, isoscaling can be restored with appropriate temperature corrections. This work was supported by the National Science Foundation under Grant Nos. PHY-95-28844 and PHY-96-05140.

Figure Caption:

Figure 1 Nuclei yield ratios are plotted as a function of N (top panels) Z (bottom panels) for central $^{124}\text{Sn} + ^{124}\text{Sn}$ and $^{112}\text{Sn} + ^{112}\text{Sn}$ collisions at $E/A = 50\text{MeV}$. The lines in the upper left panels correspond to best fits of different elements with one common slope. Similarly, in the bottom left panels, the lines correspond to fits of the same isotones. In the top right panel, the scaled isotopic ratio, $S(N)$ (Eq. 2) is constructed using $\beta = -0.417$. Similarly, in the bottom right panel, the scaled isotone ratio, $S(Z)$ defined in Eq. 3, is plotted as a function of Z using $\alpha = 0.361$.

Figure 2 Relative isotope ratios for four systems: a.) $^{16}\text{O} + ^{232}\text{Th}$ [9] and $^{16}\text{O} + ^{197}\text{Pb}$ [10] at incident energy of 137 MeV and $\theta = 40^\circ$ (upper left panel). b.) $^{14}\text{N} + ^{100}\text{Mo}$ and $^{14}\text{N} + ^{92}\text{Mo}$ at 97 MeV and $\theta = 25^\circ$ [9] (upper right panel). c.) $^{22}\text{Ne} + ^{232}\text{Th}$ and $^{22}\text{Ne} + ^{94}\text{Zr}$ at 173 MeV and $\theta = 12^\circ$ [9] (lower left panel) and d.) $^{16}\text{O} + ^{232}\text{Th}$ and $^{16}\text{O} + ^{197}\text{Au}$ at 315 MeV and $\theta = 40^\circ$ [10] (lower right panel).

Figure 3 Deviations in approximating R_{21} calculated with Eq. 7 from values calculated with Eq. 5 plotted as a function of the neutron excess for lithium to oxygen isotopes for the deeply inelastic reactions of $(N_1, Z_1) = (126, 87)$ and $(N_2, Z_2) = (150, 98)$.

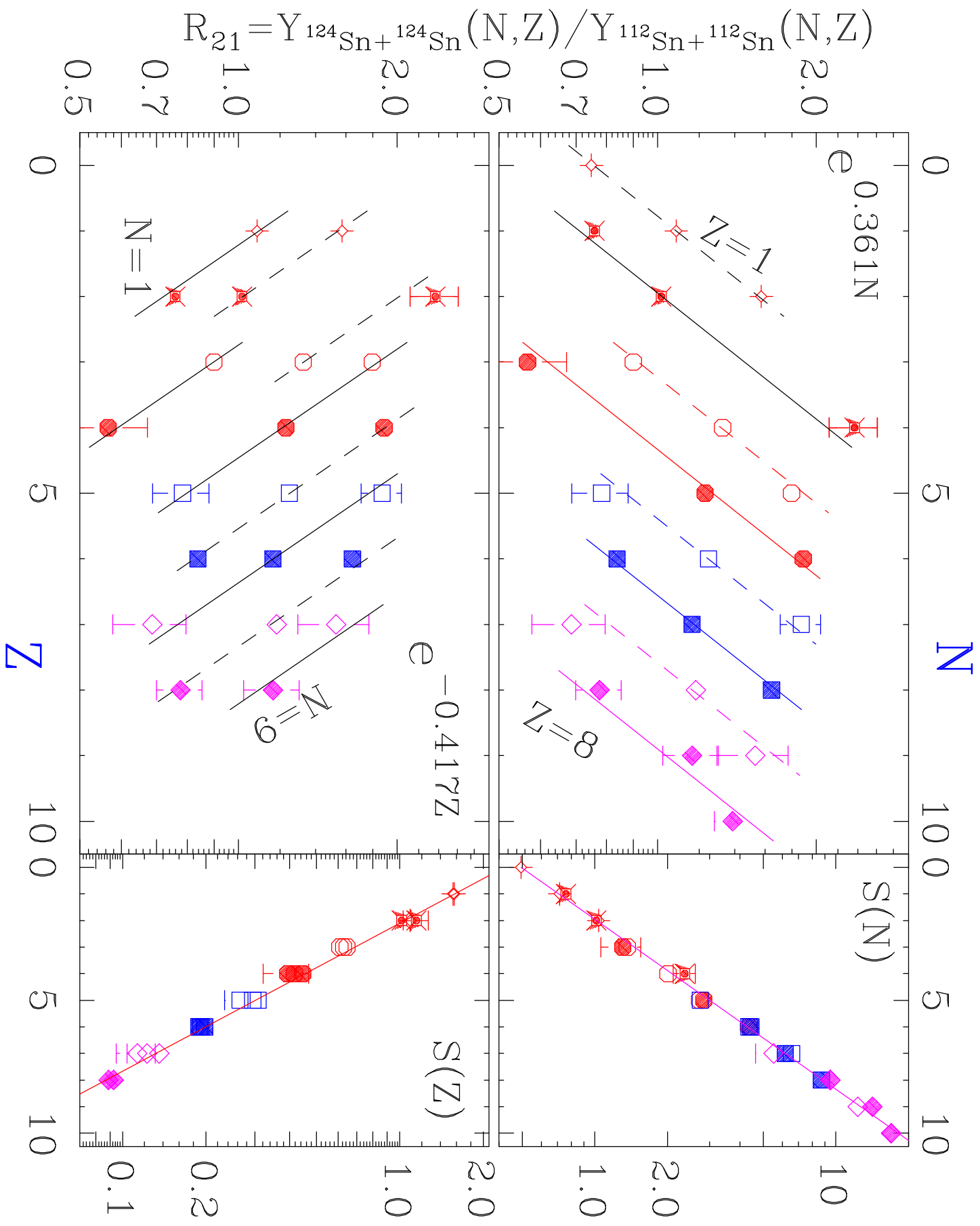
Figure 4 Relative isotope ($Z=3-6$) ratios for $^4\text{He} + ^{116}\text{Sn}$ and $^4\text{He} + ^{124}\text{Sn}$ systems emitted at backward (left panel) and forward angles (right panel). See Figures 1 and 2 for symbol conventions.

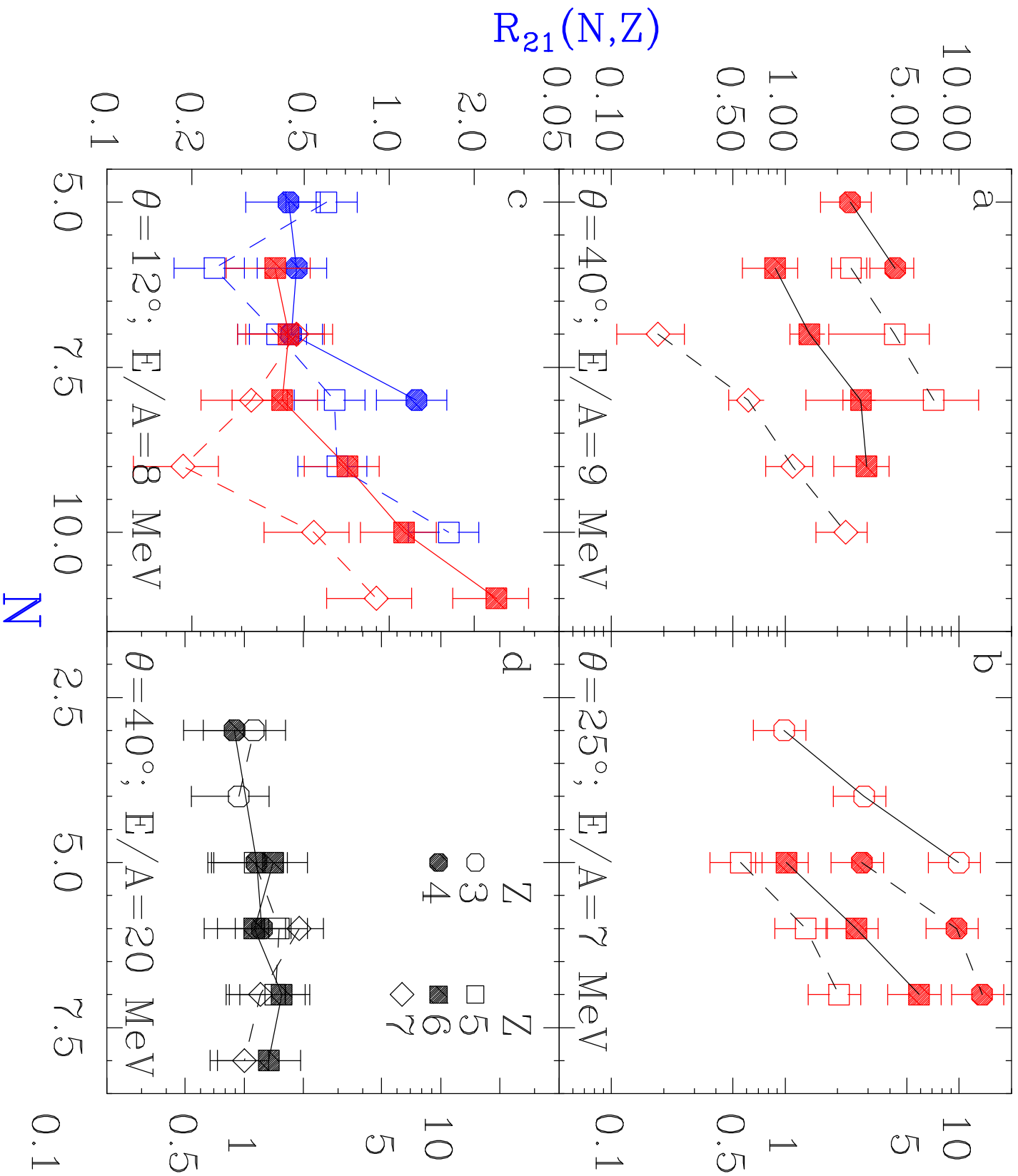
Figure 5 Left panel: Disappearance of isoscaling in reactions with different temperature. Right panel: Isoscaling is restored if the binding energy terms in the isotope ratio is corrected for the temperature difference. See Eq. (11).

References:

1. Isospin Physics in Heavy-Ion Collisions at Intermediate Energies, Eds. Bao-An Li and W. U. Schroeder, Nova Science Publishers, Inc. (2001).
2. S. Das Gupta, A.Z. Mekjian and M.B. Tsang, *Adv. Nucl. Phys.* 26 (in press) and references therein.
3. H. Müller and B. D. Serot, *Phys. Rev. C* 52, 2072 (1995).
4. H.S. Xu, M.B. Tsang, T.X. Liu, X.D. Liu, W.G. Lynch, W.P. Tan and G. Verde, L. Beaulieu, B. Davin, Y. Larochele, T. Lefort, R.T. de Souza, R. Yanez, V.E. Viola, R.J. Charity, L.G. Sobotka; *Phys. Rev. Lett.* 85, 716 (2000).
5. Bao-An Li et al., *Phys. Rev. Lett.* 78, 1644 (1997); I. Bombaci, et al., *Phys. Rep.* 242, 165 (1994); J.M. Lattimer and M. Prakash, *Ap. J.* (in press).
6. M.B. Tsang, W.A. Friedman, C.K. Gelbke, W.G. Lynch, G. Verde, H. Xu, *Phys. Rev. Lett.* 86, 5023 (2001).
7. W.P. Tan et al., MSUCL1198 (2001).
8. M.B. Tsang et al., MSUCL1203 (2001).
9. V.V. Volkov, *Phys. Rep.* 44, 93, (1978) and references therein.
10. C.K. Gelbke et. al., *Phys. Rep.* 42, 311 (1978) and references therein.
11. J.P. Bondorf, F. Dickmann, D.JH.K. Gross and P.J. Siemens, *J.de Phys.* 32, C6 (1971).
12. J. Brzychczyk et al., *Phys. Rev.* C47, 1553 (1993).
13. J. Randrup and S.E. Koonin, *Nucl. Phys. A* 356, 223 (1981);
14. S. Albergo, S. Costa, E. Costanzo, A. Rubbino, *Nuovo Cimento A* 89, 1 (1985).
15. S.R. Souza, W.P. Tan, R. Donangelo, C.K. Gelbke, W.G. Lynch, M.B. Tsang, *Phys. Rev.* C62, 064607 (2000).
16. Y. Murin et al., *Europhys. Lett.* 34, 337 (1996); Y. Murin et al., *Physca Scripta* 56, 137 (1997).
17. O.V. Lozhkin et al., *Phy. Rev. C* 46, 1996 (1992) and references therein.
18. M.B. Tsang et al., MSUCL1165 (2000).

19. M.J. Huang et al., Phys. Rev. Lett. 78, 1648 (1997).
20. H.F. Xi et al., Phys. Rev. C57, R467 (1998).
21. H. Xi et al., Phys. Lett. B431, 8 (1998).
22. G.J. Kunde, et al., Phys. Lett. B416, 56 (1998).
23. H.F. Xi et al., Phys. Rev. C58, R2636 (1998).
24. V. Serfling et al., Phys. Rev. Lett. 80, 3928 (1998).





Deviations

